Research Article | Vol. 31, No. 21 / 9 Oct 2023 / Optics Express 34313
Optics EXPRESS

# Ultrafast Yb:YAG laser oscillator with gigahertz repetition rate

MORITZ SEIDEL,* JÉRÉMIE PILAT, LUKAS LANG, CHRISTOPHER R. PHILLIPS, AND URSULA KELLER

*Institute for Quantum Electronics, ETH Zurich, 8093 Zurich, Switzerland*
*seidelm@phys.ethz.ch*

**Abstract:** We present a SESAM modelocked Yb:YAG solid-state laser providing low-noise narrowband pulses with a pulse duration of 606 fs at a 1.09-GHz repetition rate, delivering up to 2.5 W of average output power. This laser provides access to a new parameter space that could previously not be reached by solid-state lasers and, to the best of our knowledge, is the first modelocked solid-state Yb:YAG laser in the gigahertz regime. This is achieved by introducing a single additional intracavity element, specifically a nonlinear birefringent $YVO_4$ crystal, for soliton formation, polarization selection, and cavity intensity clamping. The isotropic pump absorption in Yb:YAG allows for stable and low-noise operation with multimode fiber pumping. This laser is ideally suited as a seed source for many commercial high-power Yb-doped amplification systems operating at a center wavelength around 1.03 µm. The laser exhibits a high power per comb line of 5.0 mW which also makes it interesting for applications in frequency comb spectroscopy, especially if it is used to pump an optical parametric oscillator. We measure a relative intensity noise (RIN) of 0.03%, integrated from 1 Hz to 10 MHz. Furthermore, we show that the laser timing jitter for noise frequencies >2 kHz is fully explained by a power-dependent shift in the center wavelength of 0.38 nm/W due to the quasi-three-level laser gain material. The narrow gain bandwidth of Yb:YAG reduces this contribution to noise in comparison to other SESAM modelocked Yb-doped lasers.



## 1. Introduction

Modelocked lasers with gigahertz repetition rates find many applications in optical information technology [1], ultrafast and high-precision measurements [2–4], and material processing in the ablation-cooled regime [5–8]. Several approaches for reaching these high repetition rates exist, based on fiber lasers [9], vertical cavity surface emitting lasers (VECSELs) [10] and bulk solid-state lasers. For all these technologies, cavity design limitations due to the fundamentally limited cavity length (1 GHz corresponds to a linear cavity length of 15 cm in air) need to be considered. Soliton microcombs on the other hand, due to their inherently small size, typically favor repetition rates of tens of GHz to several THz [11,12], but there have been demonstrations with repetition rates <2 GHz [13].

Modelocked fiber lasers operating in the 1-µm wavelength range usually operate at fundamental repetition rates below 1 GHz. Several challenges are involved when scaling fiber lasers to the gigahertz regime, including the need for high gain in the fiber, restricted choice of components and splices due to cavity length considerations, and Q-switching instabilities that can damage intracavity components. A fundamental repetition rate of 5 GHz has been demonstrated from a low-power non-soliton modelocked all-fiber laser [14]. However, all reported soliton modelocked fiber lasers above a 1-GHz fundamental pulse repetition rate also incorporate free-space cavity components [15,16], eliminating some of the advantages that would be offered by an all-fiber configuration. Recently, this hybrid approach of a "solid-state fiber laser" together with a rigid bonded cavity setup, has shown promising results as a low-noise, high-repetition rate (840 MHz) source [17], which operated at 1040 nm [18]. Otherwise, gigahertz repetition rate fiber lasers are

#503697 https://doi.org/10.1364/OE.503697
Journal © 2023 Received 18 Aug 2023; revised 20 Sep 2023; accepted 20 Sep 2023; published 28 Sep 2023

Optics EXPRESS

typically based on harmonic modelocking [19,20], but this typically introduces higher timing jitter noise and additional supermode noise.

Modelocked VECSELs on the other hand are naturally well suited to gigahertz repetition rates due to their sub-nanosecond-timescale carrier recombination times, and very high repetition rates above 100 GHz have been shown [21]. The same fast dynamics also suppress relaxation oscillations and associated Q-switching instabilities. However, VECSELs typically exhibit reduced efficiency when generating sub-picosecond pulses due to spectral hole burning [22].

Waveguide lasers have also been operated in the 1-μm wavelength range at gigahertz repetition rate [23]. By utilizing a waveguide and a tunable air gap, the authors obtained large nonlinearity and tunable dispersion for pulse shaping to enable a gigahertz repetition rate.

Bulk solid-state lasers have been a workhorse technology for gigahertz modelocking. An overview of selected ultrafast solid-state lasers with repetition rates >1 GHz is shown in Fig. 1(a), while a comprehensive overview can be found in [24] (Chap. 9). Earlier work with Nd-doped crystals such as Nd:$YVO_4$ enabled very high repetition rates up to 157 GHz with multi-ps-long pulses [25]. For gigahertz operation with the shortest pulses, Ti:Sapphire is the gain medium of choice due to its very broad emission bandwidth [26,27]. The gain material Er:Yb:glass has been explored extensively due to its compatibility with low-noise operation around 1550 nm for telecommunications applications. More recently, Er:Yb:glass has been utilized as a near-ideal gain medium for ultralow noise operation of gigahertz frequency combs in the femtosecond modelocking regime [28].

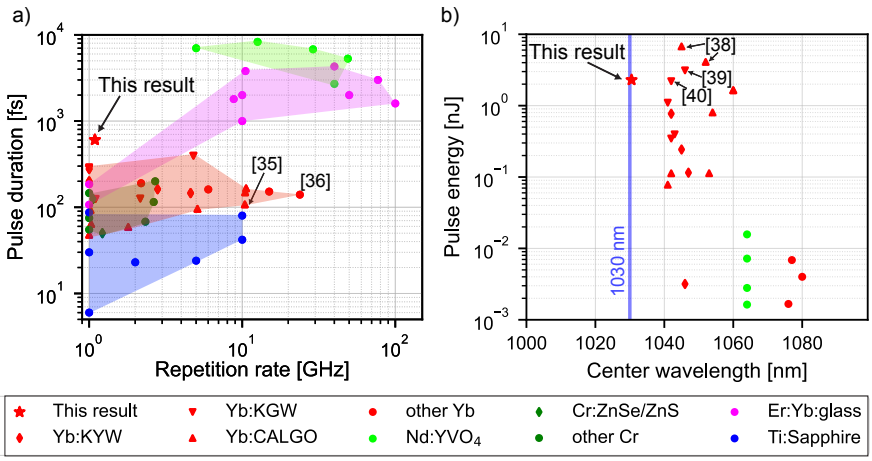


**Fig. 1.** Overview of existing ultrafast solid-state laser oscillators operating with >1 GHz repetition rate. a) Pulse duration and repetition rate for selected lasers up to 10 ps pulse duration. Different gain media and their typical operation regimes are indicated. b) Pulse energy against center wavelength for existing gigahertz lasers around 1 μm. Some results are marked with their corresponding reference numbers in the main text. References for all results shown in the graphs can be found in Supplement 1.

Around a center wavelength of 1 μm, Yb-based sources have been explored extensively due to the high efficiency and diode pumping compatibility of these lasers (see theory and examples in [24], Chap. 9). These lasers typically rely on soliton modelocking [29] with a semiconductor saturable absorber mirror (SESAM) [30] to stabilize and initiate passive modelocking. When using broadband gain media such as Yb:CALGO, Yb:KGW or Yb:KYW, these lasers reach the gigahertz regime, and optimized cavity designs have been developed to minimize the influence of Q-switching instabilities [31–33]. Such gigahertz Yb-doped lasers can provide pulse durations in the range of 100 fs with more than 1 W average power [34]. By use of gain media that support

Optics EXPRESS

pulses in the 100-fs regime, repetition rates above 10 GHz using SESAMs [35] and up to 24 GHz using Kerr-lens modelocking (KLM) [36] have been achieved.

Fig. 1(b) presents an overview of gigahertz solid-state lasers around 1 μm. To date, no high repetition rate solid-state oscillator exists that is compatible with 1030 nm. This is a significant limitation for many applications since most high-power ultrafast amplifiers operate at the Yb gain peak of 1030 nm [37]. Here, we resolve this issue by providing, to the best of our knowledge, the first gigahertz modelocked solid-state laser with a 1030-nm compatible center wavelength. The laser produces up to 2.5 W of average output power with 606-fs long pulses at a repetition rate of 1.09 GHz, resulting in a pulse energy of 2.3 nJ. As shown in Fig. 1(b), the pulse energy provided by the presented laser is competitive when comparing with other sources using different Yb-doped gain media [38–40].

An appealing application of this laser is as a pump source for a high-power high-repetition rate source. As the laser presented here uses Yb:YAG as the gain medium, it provides the center wavelength and spectral bandwidth corresponding to the most mature amplifier platforms for achieving high average output power (> 100 W) [37] as these also use Yb:YAG either in slab [41] or thin-disk architectures [42,43]. Ultrafast Yb-fiber laser systems have been operated at a variety of center wavelengths, and some prominent commercial lasers operate at 1030 nm. Optimization of the wavelength is a complex topic in these laser systems. Some considerations which favor operation at 1030 nm include pulse energy scaling [44] and transverse mode instability mitigation [45,46]. Especially interesting could be the application in burst-mode, where a train of pulses is picked from the seed laser and then amplified to be used in the ablation-cooled material processing regime [5]. When needed, pulse compression of amplified Yb lasers is now well supported via multi-pass cells [47].

When high repetition rates are required for this material processing regime, normally a low-power fiber oscillator or an electro-optic modulated frequency comb is used as the seed oscillator, often centered at 1030 nm to be compatible with the amplifier architectures. Electro-optic (EO) combs have been used to reach high repetition rates with a lot of flexibility [48,49] for exploring the materials processing parameter space. However, they do not typically provide femtosecond pulses (which are often desired for material processing) without multi-stage compression, and they have low average power (which reduces pulse contrast and requires additional amplification stages). EO combs are also complex and require significant electrical power to drive the modulators.

Ultimately, a modelocked laser such as the one presented here can provide a suitable repetition rate from a simple setup. Exhibiting high seed pulse energy and high average power, it can be easily burst-mode pulse picked and amplified for high repetition rate material processing.

For spectroscopic applications, lasers with repetition rates of a few GHz are desired, as the absorption linewidth of small molecules at ambient pressures is generally in the few-GHz regime [50]. Thus, these repetition rates offer a resolution well-matched to ambient-pressure absorption lines without requiring more complicated techniques such as spectral interleaving. Furthermore, frequency comb spectroscopic measurements generally benefit from a high power per comb line as this increases the sensitivity to weak features [51]. The laser presented here, with its 5.0 mW per comb line (average over the optical full width at half maximum), is therefore also suited for such an application, especially if combined with an optical parametric oscillator (OPO) [52] or other means for wavelength conversion. Researchers are also developing nonlinear-optics based detection techniques to enhance sensitivity, for example field-resolved spectroscopy, which uses intense near-infrared light to sample the electric field [53–55]. Another potential application area is the development of narrow-bandwidth tunable OPOs for Raman spectroscopy [56]. The oscillator presented here has high potential for these applications due to its unique combination of high repetition rate, low relative intensity noise, and compatibility with high power amplification.

In section 2 we present the laser, the modelocking results are presented in section 3, and we study the noise characteristics of the laser in section 3.1. There we present an explanation of the

Optics EXPRESS

laser's timing noise over a wide noise frequency range with a power-dependent change in the cavity round-trip time.

## 2. Experimental setup

As mentioned above, one major limitation to cavity design is the confined length of the oscillator to less than 15 cm when the desired repetition rate is above 1 GHz. The cavity configuration is shown in Fig. 2(a), with the single mode radius evolution throughout the cavity shown in Fig. 2(b).

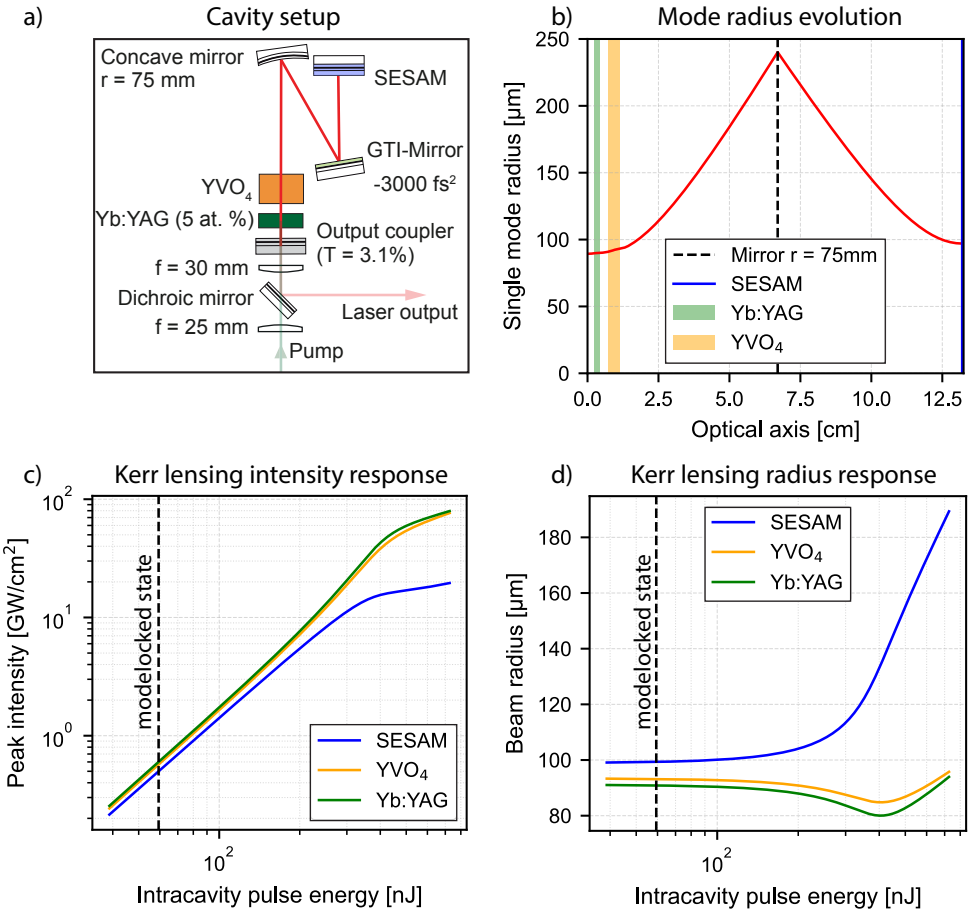


**Fig. 2.** a) Cavity design for the presented laser oscillator. The gain medium (Yb:YAG), self-phase modulation (SPM) generation material ($YVO_4$), high dispersive mirror and SESAM are indicated. b) Simulated single mode laser radius evolution throughout the cavity. c) Peak intensity on critical cavity elements (SESAM, $YVO_4$ and Yb:YAG) for a wide range of intracavity pulse energies, while taking Kerr lensing in the $YVO_4$ crystal into account. d) Resulting simulated beam radii on critical cavity elements as a function of intracavity pulse energy. The nominal fundamental modelocked operation point used for the simulation (59 nJ) is marked (dashed black line in c) and d)).

For pumping the 2-mm-long, 5 at. %-doped Yb:YAG gain crystal, a commercial VBG-stabilized multimode diode pump (DILAS IF-Series) emitting at 969 nm (zero-phonon line) is

Optics EXPRESS

used. In contrast to many gain media used for gigahertz solid-state lasers with polarization-dependent pump absorption, Yb:YAG is insensitive to pump polarization. This makes it robust against disturbances of the multimode pump delivery fiber. The pump beam is collimated with a 25-mm focal length lens and subsequently refocused using a 30-mm focal length lenses placed right in front of the output coupler (OC). The calculated minimum $1/e^2$ pump spot radius is 64 µm inside the gain medium. A dichroic OC with 3.1% transmission at 1030 nm is used and inserted between the two lenses. For stable soliton modelocking, a sufficient nonlinearity through self-phase modulation (SPM) is required. However, the comparatively long pulses provided by Yb:YAG, combined with the high repetition rate operation, result in low peak powers. This, combined with a moderate inherent nonlinearity of the gain medium at $6.13 \cdot 10^{-20}$ $m^2/W$ [57], is not sufficient to provide the nonlinearity needed for soliton modelocking [29]. Thus, a second crystal with large nonlinearity, in this case a 4-mm-long yttrium vanadate ($YVO_4$), is introduced into the cavity directly behind the gain medium and provides a nonlinearity of $15.6 \cdot 10^{-20}$ $m^2/W$ [57] along the ordinary polarization axis, resulting in a total cavity round-trip B-integral of 50 mrad at the nominal operation point. This birefringent $YVO_4$ crystal is 45° cut (with respect to its optical axis) and therefore exhibits Poynting vector walk-off. Consequently, the two polarization states are spatially separated on the gain medium and the flat OC. We use this to fix the polarization state of the laser, since only one of the two polarization states is pumped.

After a concave folding mirror with a radius of curvature of 75 mm (R > 99.9%), there is a highly dispersive mirror (Ultrafast Innovations HD73, R > 99.8%) providing −3000 $fs^2$ of group delay dispersion (GDD). The dispersive mirror was cut with a diamond saw to allow for a small angle of incidence on the concave mirror, and is placed in a custom mount. A SESAM with a strain-compensated 30 layer-pair DBR stack and a single quantum well is used as the end mirror. The SESAM, characterized with a 180-fs pulse [58], has a saturation fluence of $F_{sat} = 22$ µJ/$cm^2$, a modulation depth of 1.27% and a rollover parameter of $F_2 = 548$ mJ/$cm^2$. The recovery times of the SESAM were determined via an equivalent time sampling measurement with a 1050-nm laser [59]. A bi-exponential fit of the data yielded recovery times of $\tau_{fast} = 261$ fs and $\tau_{slow} = 3.25$ ps.

The laser mode size on the SESAM is chosen to be 95 µm ($1/e^2$ radius). The evolution of the laser mode size throughout the cavity is shown in Fig. 2(b). Through alignment of the end mirror, the polarization of the laser can be selected and switched due to the spatial walkoff present inside the birefringent crystal. For the results presented here, the polarization with no walkoff in the birefringent crystal is selected, which corresponds to s-polarization in the lab frame. The SESAM, Yb:YAG and $YVO_4$ components are mounted via custom copper mounts and are actively temperature stabilized to 25 °C, 18 °C, and 25 °C, respectively. A sheet metal box is placed around the laser to partially shield it from environmental noise sources.

One problem often encountered in high repetition rate bulk solid-state lasers is Q-switching induced damage when starting the laser, which can be exacerbated by self-focusing in the cavity. The most susceptible cavity element to this damage is the SESAM. To prevent Kerr lens induced self-focusing, the cavity can be designed such that Kerr lensing in the gain medium increases the mode size on the SESAM; this configuration thus clamps the fluence on the SESAM, preventing damage [32]. Another possibility is to introduce an additional cavity element with an effective nonlinear reflective index $n_2 < 0$, which defocusses the cavity mode on the SESAM with higher intensities. This is obtained via the cascading of quadratic nonlinearities (CQN) in the medium [33,35], and can be used to achieve repetition rates >10 GHz. CQN further provide the benefit that the self-defocusing nonlinearity is tunable.

Here, the main Kerr lens is not created by the gain medium as usual, but by the 4-mm-long $YVO_4$ crystal with its large nonlinearity that is placed in the cavity to provide most of the SPM for soliton modelocking. Thus, we carefully plan the cavity such that the $YVO_4$ crystal provides the secondary functionality of clamping the fluence on the SESAM through its Kerr

Optics EXPRESS

lens. The resulting peak intensity and cavity beam radius on the SESAM as a function of pulse energy is simulated and shown in Fig. 2(c)-(d). The simulation accounts for fundamental soliton modelocking, i.e., the pulse duration is inversely proportional to the pulse energy and the model computes the stability of soliton modelocking in comparison with continuous wave operation. At a reference point of 2-W average output power (59 nJ intracavity pulse energy), a pulse duration of 760 fs is assumed. The clamping takes effect above an intracavity pulse energy of about 300 nJ. This corresponds to an about five times higher intracavity pulse energy than in the desired modelocked state.

We use the intracavity nonlinear birefringent crystal for three purposes: soliton formation, cavity intensity clamping, and polarization selection. This has not been demonstrated before and enables a very compact, gigahertz Yb:YAG laser which avoids SESAM damage associated with transient Q-switching dynamics.

## 3. Results and discussion

To investigate the modelocking characteristics of the laser, the power is swept through the regime of stable modelocking as shown in Fig. 3(a) while monitoring the pulse duration and optical spectrum of the laser. The characteristic relation between pulse energy and pulse duration of $E_p \propto 1/\tau$ is observed, indicating soliton modelocking.

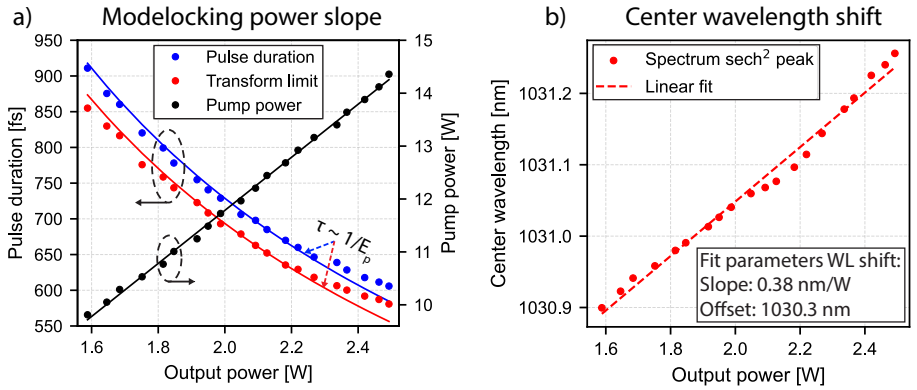


**Fig. 3.** a) Pulse duration as a function of output power as measured with an intensity autocorrelator (blue, left axis) and transform limit of the measured optical spectrum (red, left axis). Fits showing the $\tau \sim 1/E_p$ relation characteristic for soliton modelocking are shown for both measurements. Pump power as a function of output power (black, right axis) with a linear fit is also shown. b) Center wavelength shift of the optical spectrum with respect to laser output power. Data points are the maxima of sech$^2$ pulse shape fits to the optical spectra.

With varying output power of the laser, the center wavelength of the modelocked spectrum shifts as shown in Fig. 3(b). This effect is based on the fact that Yb-doped solid-state lasers are quasi-three-level lasers. As the laser power increases, the population inversion profile in the gain medium changes due to the increased optical bandwidth and saturation of the SESAM. The latter effect lowers the cavity losses until the SESAM reaches its point of maximum reflectivity. The change in population inversion leads to a change in the peak gain wavelength due to the wavelength dependence of the emission and absorption cross sections. Note that the resolution of the optical spectrum analyzer used for the experiment is 0.08 nm, but by performing sech$^2$ fits on the spectra, a more precise value for the center wavelength can be found. Performing another linear fit on the wavelength peaks of the sech$^2$ fits lead to a shift of 0.38 nm/W for this laser. The

Optics EXPRESS

narrowband gain medium results in a smaller power-dependent wavelength shift in comparison to other soliton modelocked lasers with broader gain media bandwidth [60]. Later we will relate this value back to the timing noise of the laser. During modelocked operation the laser exhibits a slope efficiency of about 20%. In continuous wave operation the laser achieved a slope efficiency of 22% using a similar cavity with a highly reflective end mirror.

The modelocking diagnostics are shown in Fig. 4 at an operation point of 2.5 W of output power. The diagnostics show that close to transform limited pulses are obtained with a time bandwidth product $<1.05 \times 0.315$. Additionally, we measure an $M^2 < 1.05$ for the laser output using a slit beam profiler.

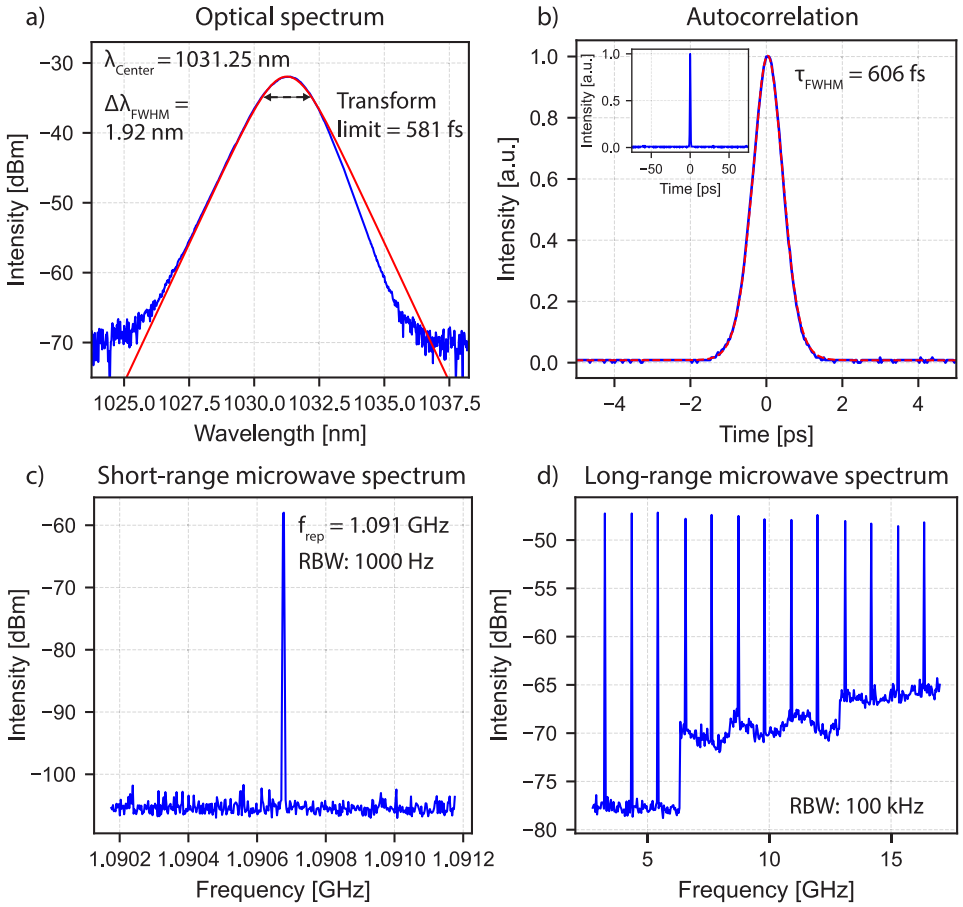


**Fig. 4.** a) Optical spectrum measured with a resolution of 0.08 nm, together with a $\text{sech}^2$ pulse shape fit, indicating a full width at half maximum (FWHM) of 1.92 nm and a corresponding transform limit of 581 fs pulses. b) Autocorrelation trace including a $\text{sech}^2$ pulse fit indicating 606 fs pulses with the inset showing a long-range autocorrelation scan over 150 ps. c) Short-range microwave spectrum with a resolution bandwidth (RBW) of 1 kHz indicating a clean microwave spectrum with a repetition rate of 1.091 GHz. d) Long-range microwave spectrum including repetition rate harmonics up to 17 GHz with a RBW of 100 kHz. The increasing noise floor is limited by the microwave spectrum analyzer.

Currently, the lasers output power is limited by the available pump power. However, for modelocking with a slow saturable absorber, the bandwidth of Yb:YAG does not support much shorter pulses than are observed at the highest available pump powers (around 600 fs) with the

Optics EXPRESS

current cavity configuration. Therefore, it is reasonable to assume that the laser is operating close to the maximum average power that can be obtained before the onset of double pulsing or continuous-wave (cw) breakthrough.

### 3.1. Noise characterization

A key consideration for many possible applications is the relative intensity noise (RIN) and timing jitter (i.e. noise in the arrival time of the modelocked pulses away from the perfect equally spaced pulse train) of the laser oscillator.

The RIN is characterized by baseband measurements on a signal source analyzer (Keysight E5052B). To cover a broad frequency range and reach a low shot-noise limit, we use the measurement technique discussed in [60] and [61]: a low-frequency measurement is performed with a transimpedance amplifier (Femto DLPCA-200), and a high-frequency measurement is performed with a voltage amplifier (Femto DUPVA-1-70). The two resulting noise power spectral densities are stitched together at 100 kHz. The result is presented in Fig. 5(a). The shot-noise of the measurement (−162.9 dBc/Hz) is calculated from the DC photocurrent of the photodiode used for the measurement (Thorlabs DET10N2).

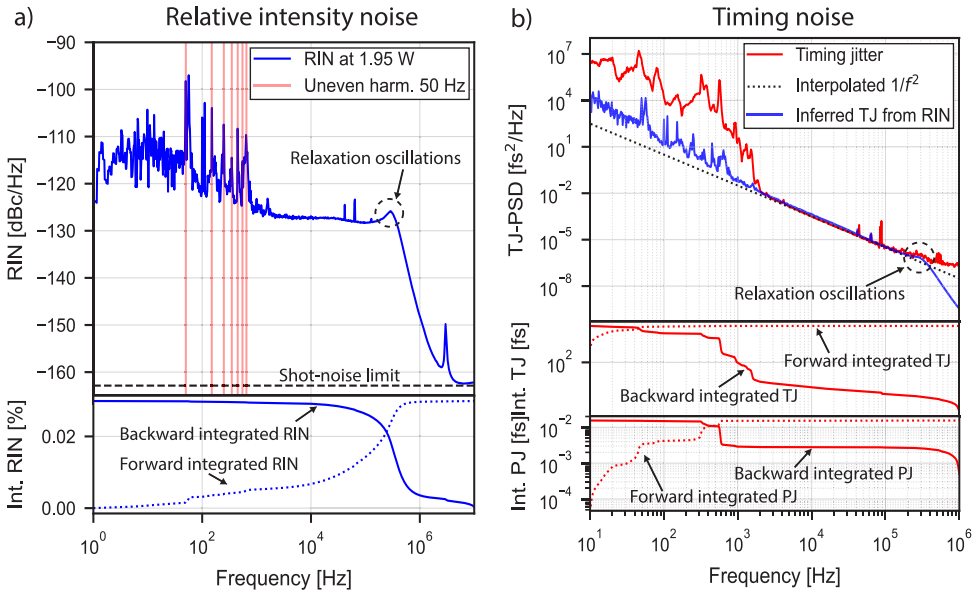


**Fig. 5.** a) One-sided relative intensity noise (RIN) power spectral density (PSD) from 1 Hz to 10 MHz with indicated shot-noise limit (-162.9 dBc/Hz) calculated from the photocurrent of the photodiode. The corresponding integrated RIN is shown below. b) One-sided timing jitter (TJ) power spectral density for noise frequencies between 10 Hz and 1 MHz inferred from phase noise measurements with the corresponding integrated timing jitter and resulting integrated period jitter (PJ). Forwards integrated RIN, TJ and PJ are integrated on the interval $[f_{\min}, f]$ (dashed lines) and backwards integrated RIN, TJ and PJ are integrated over the interval $[f, f_{\max}]$ (solid lines).

At low noise frequencies (<1 kHz) the mechanical noise contributions dominate. Apart from the mechanical noise contributions we attribute the peaks at uneven harmonics of 50 Hz to the laser diode driver. Such peaks can be suppressed by using an optimized laser diode driver, as we have done for our lab's recent dual-comb demonstrations [61]. At high noise frequencies the laser reaches the shot-noise limit. The relaxation oscillation peak is observed at around 300 kHz in the relative intensity noise spectrum. Shot-noise limited performance is achieved above 3 MHz.

Optics EXPRESS

The timing jitter of the laser is measured around the 14th harmonic of the repetition rate at 15.26 GHz, and the timing noise inferred from it (see [24], Chap. 11). The measured timing jitter power spectral density (TJ-PSD) is shown in Fig. 5(b), together with the integrated timing jitter and corresponding integrated period jitter.

Many physical processes can contribute to the TJ-PSD, including contributions relating to amplified spontaneous emission (ASE), and others relating to RIN (see [24], Chap. 11 and references therein). Several relevant processes were reviewed and summarized in [28]. These include direct timing fluctuations from ASE (section IV.A of [28]), ASE-induced central frequency shifts (section IV.B; referred to as Gordon-Haus jitter), RIN-induced self-steepening (section IV.C), and absorber saturation (section IV.D). The latter term can be generalized to account for any power-dependent change in the cavity round-trip time (starting from the derivation for absorber saturation in [62]). This results in the following contribution to the single sideband phase noise spectral density [63]:

$$L_{\mathrm{WS}}(f) = \frac{1}{2} \cdot \left( \frac{f_{\mathrm{rep}}^2}{f} \cdot \frac{\mathrm{d}\Delta t}{\mathrm{d}P} P \right)^2 \cdot S_{\mathrm{RIN}}(f) \tag{1}$$

where $S_{\mathrm{RIN}}(f)$ is the measured relative intensity noise, $f_{\mathrm{rep}}$ the repetition rate of the laser, $P$ the average output power and $\mathrm{d}\Delta t/\mathrm{d}P$ the power-dependent shift in the round-trip time as explained below.

Although self-steepening is sometimes assumed to be the dominant source, we analyzed the additional contribution due to RIN-induced center frequency shifts. To quantify this effect, we calculate the power-dependent shift in the round-trip time via the cavity GDD and the center frequency shift coefficient:

$$\frac{\mathrm{d}\Delta t}{\mathrm{d}P} = \mathrm{GDD} \cdot \frac{\mathrm{d}\omega_0}{\mathrm{d}P} \tag{2}$$

where $\omega_0$ is the center angular frequency of the laser and GDD the roundtrip group delay dispersion inside the cavity. To calculate $\mathrm{d}\omega_0/\mathrm{d}P$ we assume $\mathrm{d}\lambda/\mathrm{d}P = 0.38$ nm/W as inferred from Fig. 3(b). Fig. 5(b) shows the timing noise power spectral density predicted by Eq. (1) assuming a round-trip cavity GDD of $-4150$ fs$^2$ ($-6000$ fs$^2$ from the highly dispersive mirror and $+1850$ fs$^2$ from the crystals). The calculation, which uses the experimentally determined RIN and frequency shift, is in very good agreement with the measurements without requiring any fit parameters. The measurement and prediction differ at low frequencies due to mechanical disturbances, and at very high frequencies (> 4 MHz) due to the higher noise floor of the timing jitter measurement.

The contributions of the other noise terms discussed above (from sections IV.A – IV.D of [28]) are also calculated, but are all found to be at least 10 dB below the contribution of $L_{\mathrm{WS}}(f)$. We have observed this for other Yb-based lasers as well. This behavior can be expected for lasers based on quasi-three-level gain media since these laser systems exhibit shifts in the peak gain wavelength by the mechanism described in Section 3.

Overall, this laser exhibits 0.03% integrated RIN when integrated from 1 Hz to 10 MHz, which is comparable with other breadboard solid-state laser setups [60]. Compared to results with conventional fundamentally modelocked laser at gigahertz repetition rate employing a fiber gain segment [15], we obtain a four times lower integrated RIN. Although the mechanical noise sources have a significant influence on the integrated timing jitter at low frequencies, these noise sources would be drastically reduced by assembling the laser in a rigid prototype housing, as we have shown with our lasers before [61].

## 4. Conclusion

To the best of our knowledge, the presented laser is the first modelocked Yb:YAG oscillator with a repetition rate greater than 1 GHz. To achieve this milestone, the cavity is designed to include a

Optics EXPRESS

crystal with a large nonlinearity that provides both the required self-phase-modulation for soliton modelocking and the means to prevent damage due to catastrophic self-focusing on the SESAM. The additional birefringence of this nonlinear crystal enables linear polarization.

As this is the first modelocked gigahertz solid-state Yb:YAG laser, and in fact the first gigahertz solid-state laser operating at a center wavelength around 1030 nm, it presents an interesting source for directly seeding a high-power laser amplifier. This effort was motivated because the most widely used materials for high-power solid-state lasers and laser amplifiers exhibit gain peaks around 1030 nm [37]. Thus, this result provides a promising alternative to conventional fiber seed-oscillator based setups, enabling simpler amplification due to higher seed power and better noise performance.

For material processing applications, gigahertz burst-mode operation could be interesting, where a train of laser pulses is pulse picked (for example using an acusto-optical modulator) and subsequently amplified in bulk Yb:YAG amplification stages. After pulse picking this 2.5-W source with the typical duty-cycle of 1% for burst-mode applications, 25 mW average power remains. This can be amplified to several 10 W of average power with µJ pulses by using well established bulk Yb:YAG amplifiers [64] to obtain target parameters often used in actual applications [5], thus making this laser an exciting option for compact, low-noise gigahertz burst generation.

With the high power per comb line of 5.0 mW and the 1-GHz repetition rate this laser is also suited to high sensitivity spectroscopy measurements at ambient pressures where it combines good resolution of spectral features with great sensitivity [65]. To expand the spectroscopic abilities this laser can be used as a pump for a wavelength tunable source, or the design presented here could be further developed to allow dual-comb generation from a single cavity [66].

**Funding.** Innosuisse - Schweizerische Agentur für Innovationsförderung (40B2-0_180933); Schweizerischer Nationalfonds zur Förderung der Wissenschaftlichen Forschung (20020_200416).

**Disclosures.** The authors declare no conflicts of interest.

**Data availability.** Data underlying the results presented in this paper are not publicly available at this time but may be obtained from the authors upon reasonable request.

**Supplemental document.** See Supplement 1 for supporting content.

## References

1. P. Marin-Palomo, J. N. Kemal, and M. Karpov, *et al.*, "Microresonator-based solitons for massively parallel coherent optical communications," Nature **546**(7657), 274–279 (2017).
2. N. Picqué and T. W. Hänsch, "Frequency comb spectroscopy," Nat. Photonics **13**(3), 146–157 (2019).
3. M. Endo, A. Ozawa, and Y. Kobayashi, "6-GHz, Kerr-lens mode-locked Yb:$Lu_2O_3$ ceramic laser for comb-resolved broadband spectroscopy," Opt. Lett. **38**(21), 4502–4505 (2013).
4. T. M. Fortier, A. Bartels, and S. A. Diddams, "Octave-spanning Ti:sapphire laser with a repetition rate >1 GHz for optical frequency measurements and comparisons," Opt. Lett. **31**(7), 1011–1013 (2006).
5. C. Kerse, H. Kalaycıoğlu, and P. Elahi, *et al.*, "Ablation-cooled material removal with ultrafast bursts of pulses," Nature **537**(7618), 84–88 (2016).
6. A. Tünnermann, C. Momma, and S. Nolte, "Perspective on ultrashort pulse laser micromachining," Appl. Phys. A **129**(2), 157 (2023).
7. G. Bonamis, E. Audouard, and C. Hönninger, *et al.*, "Systematic study of laser ablation with GHz bursts of femtosecond pulses," Opt. Express **28**(19), 27702–27714 (2020).
8. H. Kalaycıoğlu, P. Elahi, and Ö. Akçaalan, *et al.*, "High-repetition-rate ultrafast fiber lasers for material processing," IEEE J. Sel. Top. Quantum Electron. **24**(3), 1–12 (2018).
9. G. Chang and Z. Wei, "Ultrafast fiber lasers: an expanding versatile toolbox," iScience **23**(5), 101101 (2020).
10. B. W. Tilma, M. Mangold, and C. A. Zaugg, *et al.*, "Recent advances in ultrafast semiconductor disk lasers," Light: Sci. Appl. **4**(7), e310 (2015).
11. T. Herr, V. Brasch, and J. D. Jost, *et al.*, "Temporal solitons in optical microresonators," Nat. Photonics **8**(2), 145–152 (2014).
12. X. Yi, Q.-F. Yang, and K. Y. Yang, *et al.*, "Soliton frequency comb at microwave rates in a high-Q silica microresonator," Optica **2**(12), 1078–1085 (2015).
13. M.-G. Suh and K. Vahala, "Gigahertz-repetition-rate soliton microcombs," Optica **5**(1), 65–66 (2018).

Optics EXPRESS


14. H. Cheng, W. Wang, and Y. Zhou, *et al.*, "5 GHz fundamental repetition rate, wavelength tunable, all-fiber passively mode-locked Yb-fiber laser," Opt. Express **25**(22), 27646–27651 (2017).
15. H.-W. Chen, G. Chang, and S. Xu, *et al.*, "3 GHz, fundamentally mode-locked, femtosecond Yb-fiber laser," Opt. Lett. **37**(17), 3522–3524 (2012).
16. I. Hartl, H. A. McKay, and R. Thapa, *et al.*, "GHz Yb-femtosecond-fiber laser frequency comb," in *Conference on Lasers and Electro-Optics/International Quantum Electronics Conference* (Optica Publishing Group, Baltimore, Maryland, 2009), p. CMN1.
17. R. Yang, M. Zhao, and X. Jin, *et al.*, "Attosecond timing jitter from high repetition rate femtosecond "solid-state fiber lasers"," Optica **9**(8), 874–877 (2022).
18. Y. Wang, H. Tian, and Y. Ma, *et al.*, "Timing jitter of high-repetition-rate mode-locked fiber lasers," Opt. Lett. **43**(18), 4382–4385 (2018).
19. Y. Deng and W. H. Knox, "Self-starting passive harmonic mode-locked femtosecond Yb3+-doped fiber laser at 1030 nm," Opt. Lett. **29**(18), 2121–2123 (2004).
20. Z. Zhao, L. Jin, and S. Y. Set, *et al.*, "2.5 GHz harmonic mode locking from a femtosecond Yb-doped fiber laser with high fundamental repetition rate," Opt. Lett. **46**(15), 3621–3624 (2021).
21. M. Mangold, C. A. Zaugg, and S. M. Link, *et al.*, "Pulse repetition rate scaling from 5 to 100 GHz with a high-power semiconductor disk laser," Opt. Express **22**(5), 6099–6107 (2014).
22. C. G. E. Alfieri, D. Waldburger, and S. M. Link, *et al.*, "Optical efficiency and gain dynamics of modelocked semiconductor disk lasers," Opt. Express **25**(6), 6402–6420 (2017).
23. S. Y. Choi, T. Calmano, and F. Rotermund, *et al.*, "2-GHz carbon nanotube mode-locked Yb:YAG channel waveguide laser," Opt. Express **26**(5), 5140–5145 (2018).
24. U. Keller, "Ultrafast Lasers," in *Graduate Texts in Physics* (Springer International Publishing, 2021).
25. L. Krainer, R. Paschotta, and S. Lecomte, *et al.*, "Compact Nd:YVO4 lasers with pulse repetition rates up to 160 GHz," IEEE J. Quantum Electron. **38**(10), 1331–1338 (2002).
26. A. Bartels, T. Dekorsy, and H. Kurz, "Femtosecond Ti:sapphire ring laser with a 2-GHz repetition rate and its application in time-resolved spectroscopy," Opt. Lett. **24**(14), 996–998 (1999).
27. H. Ostapenko, T. Mitchell, and P. Castro-Marin, *et al.*, "Design, construction and characterisation of a diode-pumped, three-element, 1-GHz Kerr-lens-modelocked Ti:sapphire oscillator," Appl. Phys. B **129**(2), 33 (2023).
28. M. Endo, T. D. Shoji, and T. R. Schibli, "Ultralow noise optical frequency combs," IEEE J. Sel. Top. Quantum Electron. **24**(5), 1–13 (2018).
29. F. X. Kartner, I. D. Jung, and U. Keller, "Soliton mode-locking with saturable absorbers," IEEE J. Sel. Top. Quantum Electron. **2**(3), 540–556 (1996).
30. U. Keller, K. J. Weingarten, and F. X. Kartner, *et al.*, "Semiconductor saturable absorber mirrors (SESAM's) for femtosecond to nanosecond pulse generation in solid-state lasers," IEEE J. Sel. Top. Quantum Electron. **2**(3), 435–453 (1996).
31. C. Hönninger, R. Paschotta, and F. Morier-Genoud, *et al.*, "Q-switching stability limits of continuous-wave passive mode locking," J. Opt. Soc. Am. B **16**(1), 46–56 (1999).
32. A. Klenner and U. Keller, "All-optical Q-switching limiter for high-power gigahertz modelocked diode-pumped solid-state lasers," Opt. Express **23**(7), 8532–8544 (2015).
33. A. S. Mayer, C. R. Phillips, and U. Keller, "Watt-level 10-gigahertz solid-state laser enabled by self-defocusing nonlinearities in an aperiodically poled crystal," Nat. Commun. **8**(1), 1673 (2017).
34. S. Pekarek, C. Fiebig, and M. C. Stumpf, *et al.*, "Diode-pumped gigahertz femtosecond Yb:KGW laser with a peak power of 3.9 kW," Opt. Express **18**(16), 16320–16326 (2010).
35. L. M. Krüger, A. S. Mayer, and Y. Okawachi, *et al.*, "Performance scaling of a 10-GHz solid-state laser enabling self-referenced CEO frequency detection without amplification," Opt. Express **28**(9), 12755–12770 (2020).
36. S. Kimura, S. Tani, and Y. Kobayashi, "Kerr-lens mode locking above a 20 GHz repetition rate," Optica **6**(5), 532–533 (2019).
37. U. Brauch, C. Röcker, and T. Graf, *et al.*, "High-power, high-brightness solid-state laser architectures and their characteristics," Appl. Phys. B **128**(3), 58 (2022).
38. M. Hamrouni, F. Labaye, and N. Modsching, *et al.*, "Efficient high-power sub-50-fs gigahertz repetition rate diode-pumped solid-state laser," Opt. Express **30**(17), 30012–30019 (2022).
39. A. Klenner, M. Golling, and U. Keller, "A gigahertz multimode-diode-pumped Yb:KGW enables a strong frequency comb offset beat signal," Opt. Express **21**(8), 10351–10357 (2013).
40. S. Pekarek, T. Südmeyer, and S. Lecomte, *et al.*, "Self-referenceable frequency comb from a gigahertz diode-pumped solid-state laser," Opt. Express **19**(17), 16491–16497 (2011).
41. P. Russbueldt, T. Mans, and J. Weitenberg, *et al.*, "Compact diode-pumped 1.1 kW Yb: YAG Innoslab femtosecond amplifier," Opt. Lett. **35**(24), 4169–4171 (2010).
42. F. Bienert, A. Loescher, and C. Röcker, *et al.*, "Experimental analysis on CPA-free thin-disk multipass amplifiers operated in a helium-rich atmosphere," Opt. Express **30**(21), 38027–38042 (2022).
43. T. Dietz, M. Jenne, and D. Bauer, *et al.*, "Ultrafast thin-disk multi-pass amplifier system providing 1.9 kW of average output power and pulse energies in the 10 mJ range at 1 ps of pulse duration for glass-cleaving applications," Opt. Express **28**(8), 11415–11423 (2020).

Optics EXPRESS


44. T. Eidam, J. Rothhardt, and F. Stutzki, *et al.*, "Fiber chirped-pulse amplification system emitting 3.8 GW peak power," Opt. Express **19**(1), 255–260 (2011).
45. C. Jauregui, C. Stihler, and J. Limpert, "Transverse mode instability," Adv. Opt. Photonics **12**(2), 429–484 (2020).
46. C. Jauregui, H.-J. Otto, and F. Stutzki, *et al.*, "Simplified modelling the mode instability threshold of high power fiber amplifiers in the presence of photodarkening," Opt. Express **23**(16), 20203–20218 (2015).
47. A.-L. Viotti, M. Seidel, and E. Escoto, *et al.*, "Multi-pass cells for post-compression of ultrashort laser pulses," Optica **9**(2), 197–216 (2022).
48. H. Ye, F. Leroi, and L. Pontagnier, *et al.*, "High-power nonlinear amplification of an ultrafast electro-optic frequency comb with flexible GHz repetition rate," Opt. Express **30**(7), 10605–10613 (2022).
49. H. Ye, L. Pontagnier, and C. Dixneuf, *et al.*, "Multi-GHz repetition rate, femtosecond deep ultraviolet source in burst mode derived from an electro-optic comb," Opt. Express **28**(25), 37209–37217 (2020).
50. C. R. Phillips, B. Willenberg, and A. Nussbaum-Lapping, *et al.*, "Coherently averaged dual-comb spectroscopy with a low-noise and high-power free-running gigahertz dual-comb laser," Opt. Express **31**(5), 7103–7119 (2023).
51. P. Maslowski, K. F. Lee, and A. C. Johansson, *et al.*, "Surpassing the path-limited resolution of Fourier-transform spectrometry with frequency combs," Phys. Rev. A **93**(2), 021802 (2016).
52. C. P. Bauer, S. L. Camenzind, and J. Pupeikis, *et al.*, "Dual-comb optical parametric oscillator in the mid-infrared based on a single free-running cavity," Opt. Express **30**(11), 19904–19921 (2022).
53. I. Pupeza, M. Huber, and M. Trubetskov, *et al.*, "Field-resolved infrared spectroscopy of biological systems," Nature **577**(7788), 52–59 (2020).
54. I. Pupeza, D. Sánchez, and J. Zhang, *et al.*, "High-power sub-two-cycle mid-infrared pulses at 100 MHz repetition rate," Nat. Photonics **9**(11), 721–724 (2015).
55. P. Sulzer, M. Högner, and A.-K. Raab, *et al.*, "Cavity-enhanced field-resolved spectroscopy," Nat. Photonics **16**(10), 692–697 (2022).
56. B. Sophie, F. Patrick, and W. Nico, *et al.*, "Optical parametric oscillator-based light source for coherent Raman scattering microscopy: practical overview," J. Biomed. Opt. **16**(02), 021106 (2011).
57. P. Kabaciński, T. M. Kardaś, and Y. Stepanenko, *et al.*, "Nonlinear refractive index measurement by SPM-induced phase regression," Opt. Express **27**(8), 11018–11028 (2019).
58. D. J. H. C. Maas, B. Rudin, and A. R. Bellancourt, *et al.*, "High precision optical characterization of semiconductor saturable absorber mirrors," Opt. Express **16**(10), 7571–7579 (2008).
59. A. Nussbaum-Lapping, C. R. Phillips, and B. Willenberg, *et al.*, "Absolute SESAM characterization via polarization-resolved non-collinear equivalent time sampling," Appl. Phys. B **128**(2), 24 (2022).
60. S. L. Camenzind, T. Sevim, and B. Willenberg, *et al.*, "Free-running Yb:KYW dual-comb oscillator in a MOPA architecture," Opt. Express **31**(4), 6633–6648 (2023).
61. J. Pupeikis, B. Willenberg, and S. L. Camenzind, *et al.*, "Spatially multiplexed single-cavity dual-comb laser," Optica **9**(7), 713–716 (2022).
62. R. Paschotta, "Noise of mode-locked lasers (Part II): timing jitter and other fluctuations," Appl. Phys. B **79**(2), 163–173 (2004).
63. "IEEE standard definitions of physical quantities for fundamental frequency and time metrology–random instabilities," *IEEE Std 1139-2008* (Revision of IEEE Std 1139-1999), 1–50 (2009).
64. P. Russbueldt, T. Mans, and G. Rotarius, *et al.*, "400 W Yb:YAG Innoslab fs-amplifier," Opt. Express **17**(15), 12230–12245 (2009).
65. C. P. Bauer, J. Pupeikis, and B. Willenberg, *et al.*, "High-sensitivity dual-comb spectroscopy in the SWIR using a widely-tunable, free-running spatially-multiplexed dual-comb optical parametric oscillator," arXiv, arXiv:2305.02908 (2023).
66. B. Willenberg, J. Pupeikis, and L. M. Krüger, *et al.*, "Femtosecond dual-comb Yb:CaF2 laser from a single free-running polarization-multiplexed cavity for optical sampling applications," Opt. Express **28**(20), 30275–30288 (2020).